IOP Publishing Journal of Physics: Condensed Matter
J. Phys.: Condens. Matter **32** (2020) 195804 (7pp) https://doi.org/10.1088/1361-648X/ab686c

Transition metal substituted Fe_2P: potential candidate for MRAM application

Soumya S Bhat, Enamullah, Seung-Cheol Lee and Satadeep Bhattacharjee

Indo-Korea Science and Technology Center (IKST), Bangalore 560065, India

E-mail: seungcheol.lee@ikst.res.in and satadeep.bhattacharjee@ikst.res.in

Received 1 October 2019, revised 2 December 2019
Accepted for publication 7 January 2020
Published 13 February 2020

Abstract

We propose transition metal substituted Fe_2P as a new promising material for spin-transfer torque magnetic random-access memory (STT-MRAM) application. Using first-principles calculations based on density functional theory and Monte Carlo simulations, we demonstrate that this material can be used as a ferromagnetic electrode in the magnetic tunnel junction (MTJ) of STT-MRAM due to its moderate perpendicular magnetic anisotropy, high ferromagnetic transition temperature, and large tunnel magnetoresistance. This work is expected to provide a basis for the development of a new class of Fe_2P-based electrode materials for STT-MRAM devices.

Keywords: transition metal phosphides, magnetocrystalline anisotropy, magnetic tunnel junction, tunnel magnetoresistance, density functional theory calculations

(Some figures may appear in colour only in the online journal)

1. Introduction

Over the last two decades, spin-transfer torque magnetic random-access memory (STT-MRAM) has received increasing attention and has been the focus of spintronics research. Due to their high density, low power consumption, and non-volatility, STT-MRAMs are considered to be one of the promising contenders for next-generation universal memory [1]. The basic unit of a STT-MRAM is magnetic tunnel junction (MTJ), which comprises a thin non-magnetic insulating layer sandwiched between two ferromagnetic layers. For a technologically efficient MTJ, high tunnel magnetoresistance (TMR) ratio, low switching current, and high thermal stability are the key requirements [2, 3]. High TMR ratios were reported for MgO-based MTJs with FeCo, FeCoB and FePt electrodes [4, 5]. Despite the success of these electrode materials, there is still a need for exploring a variety of materials. In the present study, we investigate the feasibility of transition metal (TM) substituted Fe_2P in pursuit of a new class of electrode materials for the STT-MRAM application.

Fe_2P stands out as a particularly interesting material, due its known sufficiently large value of saturation magnetic moment and large magnetocrystalline anisotropy energy (MAE) [6]. In addition Fe_2P is composed of low-cost and widely available elements. However, due to its low Curie temperature (T_C) of 216 K [7], stoichiometric Fe_2P is impractical for room temperature applications. Earlier studies have shown great enhancement in T_C, either by substitution on Fe or on P sites [7–10], making them useful for room temperature applications. Interesting magnetic behaviour have been reported for Mn, Cr, Co and Ni substitutions of Fe_2P using Mössbauer spectroscopy [7, 11–15]. Very small substitutions of Mn, $(Fe_{1-x}Mn_x)_2P$ (for $x < 0.015$) induce metamagnetism and for $x > 0.03$ it is antiferromagnetic. Similar results are reported for Cr substitution [7, 14]. Contrary to Mn and Cr substitutions, addition of Co in Fe_2P enhances T_C to a maximum of 480 K at $x = 0.3$ [13]. Similar behaviour is observed for $(Fe_{1-x}Ni_x)_2P$ compounds with T_C reaching to maximum (342 K) at about $x = 0.1$ [14, 16]. Further, presence of very small amount of Cu impurities are found to greatly enhance the T_C [17]. Besides, substituting P with B, Si and As significantly increases the T_C [8–10].

Due to simplicity in the synthesis and abundance of material, magnetic applications frequently make use of Fe-based alloys. Given its importance, many theoretical and experimental efforts are devoted to studying the structural and

Table 1. Calculated local and total magnetic moment (in μ_B f.u.$^{-1}$)) for Fe_2P and $(Fe_{1-x}M_x)_2P$, $x = 1/6$. μ_{Fe_I} and $\mu_{Fe_{II}}$ are average local magnetic moment at Fe_I and Fe_{II} sites, respectively. μ_M represents local magnetic moment of M atom substituted at Fe_I or Fe_{II} sites.

	Site	μ_{Fe_I}	$\mu_{Fe_{II}}$	μ_M	μ_{total}
Fe_2P	—	0.83	2.23	—	3.01
$(Fe_{1-x}Co_x)_2P$	Fe_I	0.75	2.13	0.37	2.71
	Fe_{II}	0.88	2.30	0.87	2.66
$(Fe_{1-x}Ni_x)_2P$	Fe_I	0.59	2.03	0.12	2.43
	Fe_{II}	0.88	2.18	0.28	2.39
$(Fe_{1-x}Cu_x)_2P$	Fe_I	0.42	1.90	0.004	2.15
	Fe_{II}	0.82	1.93	0.04	2.07
$(Fe_{1-x}Zn_x)_2P$	Fe_I	0.27	1.75	−0.04	1.88
	Fe_{II}	0.77	1.53	−0.12	1.75

magnetic properties of Fe_2P-based alloys. However no efforts have been made so far in a direction where non-stoichiometric Fe_2P may find a 'softer' magnetic application such as switching component [18–21] in magnetic devices. In the present study, we rationalize the attainability of such an application.

In the first part of this work, we examine the effect of Co, Ni, Cu and Zn substitution on the magnetic moment and MAE of Fe_2P using first-principles calculations based on density functional theory (DFT). In the second part, we investigate its potential for MRAM application through the calculation of T_C and TMR ratios, considering Cu substituted Fe_2P as an exemplar. We discuss our findings following a brief outline of the computational methods.

2. Computational details

We performed first-principles calculations using the projector-augmented wave (PAW) method [22] in the framework of DFT as implemented in VASP code [23, 24]. The exchange-correlation energy of electrons is treated within a generalized gradient approximated functional (GGA) of the Perdew–Burke–Ernzerhof (PBE) [25] parameterized form. Interactions between ionic cores and valence electrons are represented using PAW pseudo-potentials, where 4*s*, 3*d* electrons for TMs (Fe, Co, Ni, Cu, and Zn) and 3*s*, 3*p* electrons for P are treated as valence. Plane-wave basis set with a kinetic energy cutoff of 500 eV and an energy convergence criteria of 10^{-6} eV are used. A uniform mesh of $9 \times 9 \times 5$ k-points used for Brillouin zone sampling of the unit cell provided sufficient accuracy. The MAE is calculated using magnetic force theorem given by,

$$\mathrm{MAE} = \sum_{i}^{\mathrm{occ}} \sum_{k} \varepsilon(\hat{\mathbf{e}}_{\mathrm{hard}}, k) - \sum_{i}^{\mathrm{occ}} \sum_{k} \varepsilon(\hat{\mathbf{e}}_{\mathrm{easy}}, k) \qquad (1)$$

where $\varepsilon(\hat{\mathbf{e}}_{\mathrm{hard/easy}}, k)$ is energy of the i^{th} band when the magnetization is pointed either along the hard/easy direction. Heisenberg exchange coupling constants (J_{ij}) are calculated using spin-polarized relativistic (SPR) Korringa–Kohn–Rostoker (KKR) Green's function method, as implemented within SPRKKR package [26]. Using the Heisenberg model, exchange Hamiltonian is given by,

$$\hat{H} = -\sum_{i \neq j} J_{ij} \hat{e}_i \hat{e}_j, \qquad (2)$$

where, $\hat{e}_i$ and $\hat{e}_j$ are the unit vectors along the direction of local magnetic moment on atomic site *i* and *j* respectively. The exchange parameters can be obtained from the energy difference between two different magnetic configurations using the formulation of Liechtenstein *et al* [27]. An angular momentum cutoff of $l_{\max} = 3$ and 30 complex energy points are used for the expansion of Green's function. The energy convergence criteria of 10^{-5} is used for self-consistent cycles. Equilibrium lattice parameters obtained from the *ab initio* simulation are used to calculate exchange interaction parameters.

Curie temperature (T_C) is obtained from the Monte Carlo (MC) simulation using uppsala atomistic spin dynamics (UppASD) package [28], where we use the Hamiltonian in the following form,

$$\mathcal{H} = -\sum_{ij} J_{ij} \mathbf{e}_i \mathbf{e}_j - K_u \sum_{i} (\mathbf{e}_i \cdot \mathbf{e})^2 \qquad (3)$$

where **e** is the unit vector along the direction of the easy axis and K_u is the uniaxial anisotropy constant which are reported in table 2. We have used a $12 \times 12 \times 12$ supercell with periodic boundary condition. At each temperature, 25 000 MC steps are performed for equilibration using the magnetic configuration of the previous temperature as the starting point. After the equilibration, the measurements are performed by using additional 50 000 MC steps.

Table 2. Calculated MAE(in MJ m^{-3}) along with magnetic easy and hard axes for Fe_2P and $(Fe_{1-x}M_x)_2P$ with $x = 1/6$.

	Site	Easy axis	Hard axis	MAE
Fe_2P	—	001	100	2.38
$(Fe_{1-x}Co_x)_2P$	Fe_I	001	100	0.96
	Fe_{II}	001	100	0.91
$(Fe_{1-x}Ni_x)_2P$	Fe_I	100	010	0.47
	Fe_{II}	001	100	0.70
$(Fe_{1-x}Cu_x)_2P$	Fe_I	100	001	1.26
	Fe_{II}	001	100	0.87
$(Fe_{1-x}Zn_x)_2P$	Fe_I	100	001	0.62
	Fe_{II}	001	100	0.74

3. Results and discussion

Initial structure of Fe_2P is taken from the experimental data [29] and is optimized by full relaxation of the unit cell and atomic positions. Fe_2P crystallizes in hexagonal C22 structure with space group $P\bar{6}2m$ [30]. The unit cell is composed of three formula units with three Fe atoms occupying 3*f* sites (Fe_I), remaining three Fe atoms in 3*g* sites (Fe_{II}), two P atoms occupying 2*c* sites (P_I) and one P atom in 1*b* site (P_{II}). Fe_I

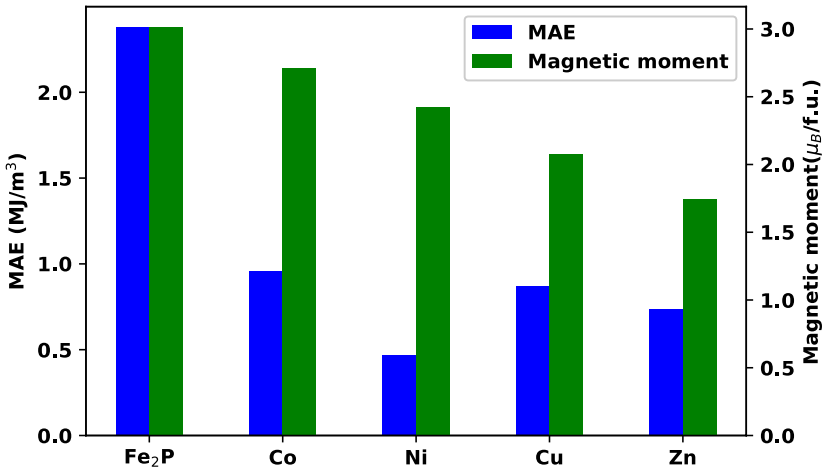

Figure 1. Calculated MAE and magnetic moment for pristine and TM substituted Fe_2P.

atom is surrounded by four P atoms, whereas Fe_{II} atom is surrounded by five P atoms, and so referred as tetrahedral and pyramidal sites, respectively. Computed lattice constants ($a = 5.81$ and $c = 3.43$ Å) agree well with the reported experimental values ($a = 5.87$, and $c = 3.46$ Å) [29].

An early x-ray diffraction experiment on $(Fe_{1-x}M_x)_2P$ alloys (where M is a TM) by Fruchart *et al* [7] revealed Fe_2P-type hexagonal structure for $x \leqslant 0.2$. Therefore, we took the optimized nine-atom basis cell of Fe_2P and one out of six Fe atoms, either from Fe_I site or Fe_{II} site is substituted by a TM resulting in the formula $(Fe_{1-x}M_x)_2P$, with $x = 1/6$ and M = Co, Ni, Cu and Zn. To examine the site preference of the solute M atoms in $(Fe_{1-x}M_x)_2P$, we compared the total energies for both cases, i.e. with M atom at Fe_I and Fe_{II} sites. For $(Fe_{1-x}Co_x)_2P$, total energy is lower by 67 meV f.u.$^{-1}$ when Co occupies Fe_I site. This is in agreement with the earlier Mössbauer studies [7, 31] which disclosed the preferential filling of tetrahedral site. Same trend is obtained for Ni substitution where the energy difference is 21 meV f.u.$^{-1}$, which is in accordance with the experimental finding, where Ni atoms occupy Fe_I site preferentially, for x in the range $0 \leqslant x \leqslant 0.3$, but Fe_{II} site for $x > 0.7$ [7, 12, 32]. In case of $(Fe_{1-x}Cu_x)_2P$ and $(Fe_{1-x}Zn_x)_2P$, our calculations predict that Cu and Zn substitutes Fe preferentially at pyramidal site, for which there are no previous data available for comparison.

3.1. Magnetic moment and anisotropy

Table 1 presents the total and local magnetic moments calculated for 3*f* and 3*g* sites for Fe_2P and $(Fe_{1-x}M_x)_2P$. Calculated total magnetic moment for Fe_2P (3.01 μ_B f.u.$^{-1}$) agrees well with the experimental value (3.27 μ_B) [33]. The local magnetic moments computed for 3*f* and 3*g* sites (0.83 and 2.23 μ_B) are also in accordance with earlier reports (0.96 and 2.31 μ_B f.u.$^{-1}$) [33]. For Co substitution total magnetic moment decreases to 2.71 μ_B f.u.$^{-1}$, which is comparable with the experimental value of 2.47 μ_B f.u.$^{-1}$ reported for $(Fe_{0.70}Co_{0.30})_2P$ measured at 12 K [15]. For Ni substitution, computed value is 2.43 μ_B f.u.$^{-1}$, which is consistent with the experimental value of 2.14 μ_B f.u.$^{-1}$ measured at 4 K for $(Fe_{0.75}Ni_{0.25})_2P$ [12]. The agreement between our calculation and experimental values are acceptable as magnetic moments are found to decrease monotonically with increase in x, for Co and Ni substitutions [12–14]. The predicted μ_{total} for Cu and Zn substitutions are 2.07 and 1.75 μ_B f.u.$^{-1}$, respectively. Table 2 lists the MAE estimated for pristine and TM substituted Fe_2P. For Fe_2P, computed MAE is 2.38 MJ m^{-3}, which is very close to experimentally determined value of 2.32 MJ m^{-3} measured at low-temperature [34]. Further, our calculation reproduces the observed *c*-axis as the magnetization easy axis. From table 2 it is evident that for all TM substitutions, the calculated MAE is lower than that of Fe_2 P. Kumar *et al* [13] reported the decrease in MAE for Co substitution up to 10% in the hexagonal phase and then progressive increase with increasing Co in the orthorhombic phase. For Ni substitution, Fujii *et al* [14] through their experiments revealed a monotonic decrease in MAE with increase in x and dropping to zero at $x = 0.3$. Thus, our results are in accordance with these experimental findings. For Cu and Zn substitutions there are no previous experimental reports available and our calculations predict their MAE to be 0.87 and 0.74 MJ m^{-3}, respectively. Figure 1 illustrates the variation of MAE and total magnetic moment for Fe_2P and $(Fe_{1-x}M_x)_2P$. As seen from the figure total moment decreases linearly as we move from Fe to Zn, and MAE is reduced for all TM substitutions. The decrease in MAE of Fe_2P due to TM substitutions can be explained in terms of optimal band filling as MAE is known to be predominantly influenced by band filling. The MAE reaches its peak value close to the electron count corresponding to pure Fe_2P and decreases as it deviates from the optimal electron count. This is explained in detail by Zhuravlev *et al* [35], where they discuss the strategy for maximizing the magnetocrystalline anisotropy by tuning the alloy content of Fe_2P. Similar to Fe_2P, lower energy structures of TM substituted Fe_2P also have [0 0 1] as magnetization easy axis. Since these alloys have T_C above room temperature [13, 14, 16, 17] and magnetic easy axis oriented along [0 0 1] direction, they can be used in perpendicular magnetic recording applications. From the above discussions, it is quite evident that TM substituted Fe_2P could be a potential candidate for the MRAM application. In the next sections, we

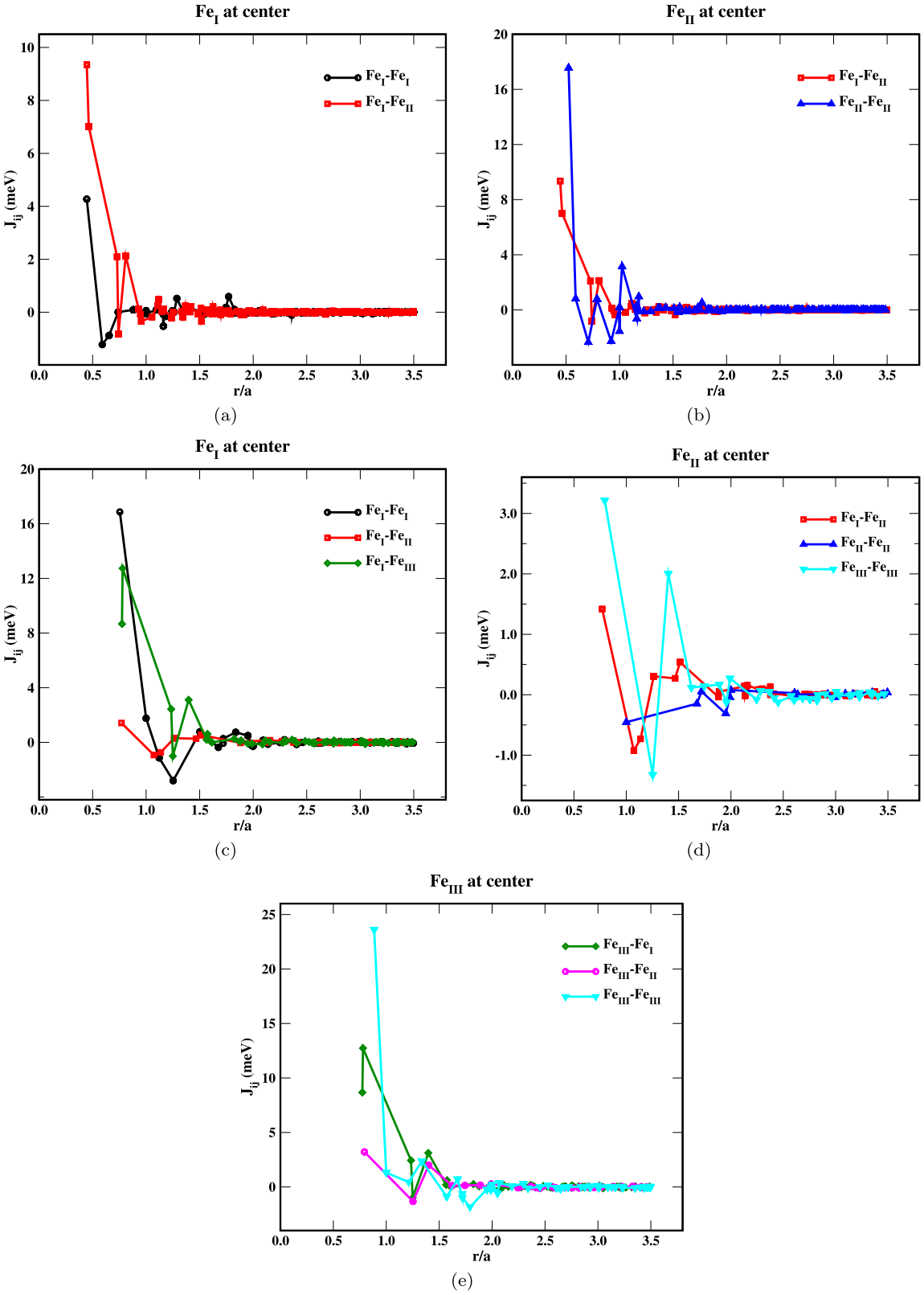

Figure 2. Calculated exchange constants for Fe_2P (a)–(b) and $(Fe_{1-x}Cu_x)_2P$ (c)–(e).

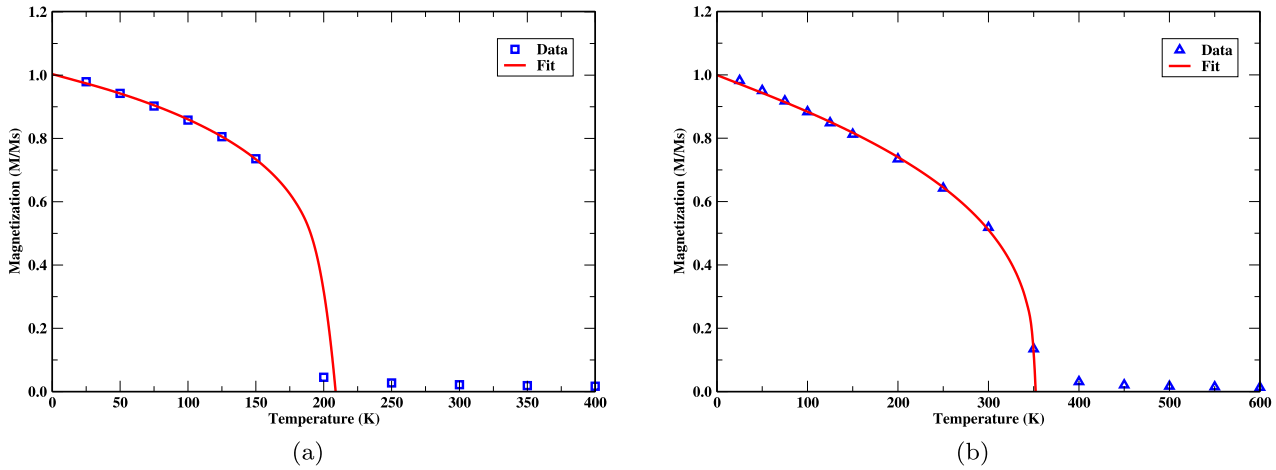

Figure 3. Monte Carlo simulation for temperature dependent magnetization (normalized to saturation magnetization) as a function of temperature for (a) Fe_2P and (b) $(Fe_{1-x}Cu_x)_2P$.

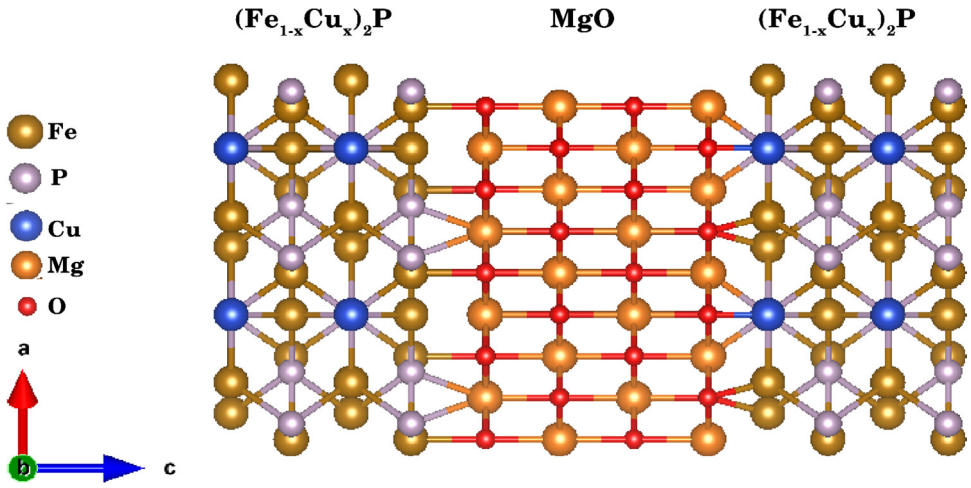

Figure 4. Ball and stick model of magnetic tunnel junction consisting of $(Fe_{1-x}Cu_x)_2P$ and MgO.

further investigate its competence for the same by determining T_C and TMR ratios, considering Cu substituted Fe_2P as an exemplar.

3.2. Exchange interaction constants and T_C

Results of interatomic exchange constants for pristine and Cu-substituted Fe_2P obtained using the SPR-KKR package as a function of distance are shown in figure 2. Using calculated magnetic moments and exchange constants as input data, MC simulations are performed by employing the metropolis algorithm. The transition probability between two states (s and s') in Markov chain $W(s \to s')$ is represented by $W(s \to s') = \min\left\{1, e^{-\frac{\Delta E}{K_B T}}\right\}$, $\Delta E = E_{s'} - E_s$ is the difference in energy of the corresponding states. The simulated temperature-dependent normalized magnetization plots for pure and Cu substituted Fe_2P are shown in figure 3. The obtained data points are fitted using the Curie-Bloch equation [36] given by,

$$m(\tau) = (1 - \tau^{\gamma})^{\beta}, \tag{4}$$

where $\tau = \frac{T}{T_C}$ is the reduced temperature, γ a phenomenological constant, and β is the critical exponent. The choice of equation (4) stems from the fact that Fe_2P related systems do not behave like pure classical magnets [30]. In the limit, $\gamma = 1$, the equation (4) reduces to one which is usual for a classical ferromagnet. The fitted value of T_C for Fe_2P is 207 K, which is in good agreement with the experimental value of 216 K [7], and that for Cu-substituted Fe_2P is 353 K (see figure 3). Although previous experiments revealed an increase in T_C of Fe_2P due to the presence of Cu impurities [17], quantifiable results are not available in the literature. The origin of the larger value of T_C for Cu-substituted Fe_2P can be understood from figure 2. It can be seen that for the pure case, the strongest interaction is Fe_{II}–Fe_{II} type and is about 17 meV. The major interaction between the two different Fe sublattices, viz. between Fe_I and Fe_{II} is about 9 meV. While in the case of Cu-substituted Fe_2P, there are three irons (Fe_I, Fe_{II}, Fe_{III}), among which the most prominent interaction is between the Fe_{III} sites which is about 24 meV. Also, there is a relatively stronger inter-sublattice

Table 3. TMR ratios estimated for pristine and Cu-substituted Fe_2P MTJ for different number of MgO insulating layers.

	TMR ratio (%)	
No. of MgO layers	Fe_2P	$(Fe_{1-x}Cu_x)_2P$
2	64	97
4	54	109
6	58	122

interaction (between Fe_I and Fe_{III}) about 12 meV. It is to be noted that in both cases, intra-sublattice exchange interaction plays a dominant role.

We have also determined Gilbert damping parameter, α for bulk pristine and Cu-substituted Fe_2P. The magnetic damping parameter is an important factor in determining the performance of magnetic devices. A high damping parameter is essential for devices requiring high switching speeds [37], whereas low value is desired to achieve low critical switching current. The calculation of α is based on the *ab initio* Green's function technique and linear response formalism as implemented in SPRKKR package. We have used a k-point grid consisting of 2800 points in the irreducible Brillouin zone for the self-consistent calculation, while a much denser grid with 800 000 points is used for the calculation of α. The effect of finite temperatures on α is treated using an alloy-analogy model which deals with the thermal displacement of atoms in a quasi-static manner. The α of pristine and Cu-substituted Fe_2P computed at 60 K is 0.032 and 0.038, respectively. Note that in the present work we have calculated intrinsic contribution to the damping. However, in practical applications, extrinsic contributions caused by spin pumping [38] or modified electronic structure at the interface may dominate the damping [39].

3.3. Tunnel magnetoresistance (TMR)

MTJs consisting of MgO as an insulating barrier, with varying thicknesses (2, 4 and 6 atomic layers) sandwiched between pristine or Cu-substituted Fe_2P layers are considered for the estimation of TMR ratios. A supercell approach is used and MgO(0 0 1) is rotated by 45° with respect to Fe_2P(0 0 1) to match the lattice. The in-plane lattice parameter of the supercell is fixed to that of Fe_2P and therefore MgO experiences a strain of ∼5%. Figure 4 shows schematic of modelled $(Fe_{1-x}Cu_x)_2P$(0 0 1)/MgO(0 0 1)/$(Fe_{1-x}Cu_x)_2P$(0 0 1) MTJ. TMR ratios are estimated using Julliere's model [40] which correlates TMR and polarization by the relation,

$$\mathrm{TMR} = \frac{2P_1P_2}{1 - P_1P_2} \tag{5}$$

where, P_1 and P_2 are spin polarization values of left and right electrodes respectively. P is calculated from the spin dependent density of states n at the fermi energy E_F using the equation,

$$P = \frac{n_\uparrow(E_F) - n_\downarrow(E_F)}{n_\uparrow(E_F) + n_\downarrow(E_F)}. \tag{6}$$

Calculated TMR ratios for pristine and Cu-substituted Fe_2P for varied MgO layer thicknesses are listed in table 3. As apparent from the table, TMR ratios of Fe_2P are almost doubled with Cu substitution. For $(Fe_{1-x}Cu_x)_2P$ with six atomic layers of MgO, a TMR ratio as large as ∼120% is obtained. Earlier studies involving perpendicular CoFeB/MgO systems have demonstrated higher TMR ratios along with reasonable STT switching critical current density and faster switching speeds [41–45]. Recently TMR ratio as high as 249% has been achieved for a bottom-pinned perpendicular-MTJ stack with atom-thick W layers and double MgO/CoFeB interfaces patterned into nanopillars [46]. While the TMR ratio presented in this work is comparatively low, it could be enhanced by selecting the appropriate spacer, bridging [46] and capping layers [47] with suitable thicknesses. Hence, from our calculations, we predict that TM substituted Fe_2P could be a promising candidate for the STT-MRAM application. We are not aware of any published report on the use of Fe_2P-based materials towards this application, and the results presented here may provide the basis for further development of a new class of electrode materials for MTJs.

4. Conclusions

In summary, we have studied the magnetic properties of TM substituted Fe_2P using first-principles calculations based on DFT. Our calculations show that Co, Ni substitutes Fe preferentially at the tetrahedral site, whereas Cu and Zn substitute at the pyramidal site. For all TM substitutions, the total magnetic moment is less than that of pristine Fe_2P and decreases linearly as we move from Co to Zn substitution. Fe_2P retains [0 0 1] as magnetization easy axis for TM substitutions, however, it shows a reduction in MAE. For Cu-substituted Fe_2P, T_C is calculated to be 353 K. TMR ratio as large as ∼120% is predicted for MTJ with MgO as an insulating barrier. Our calculations thus disclose the significant potential of TM substituted Fe_2P to be used as a component for STT-MRAM. The results presented here may serve as a groundwork for more detailed experimental and theoretical efforts towards Fe_2P-based materials for MRAM application.

Acknowledgment

We acknowledge support from the Convergence Agenda Program (CAP) of the Korea Research Council of Fundamental Science and Technology (KRCF) and Global Knowledge Platform (GKP) program of the Ministry of Science, ICT and Future Planning.

ORCID iDs

Soumya S Bhat https://orcid.org/0000-0002-1624-2712
Seung-Cheol Lee https://orcid.org/0000-0002-9741-6955
Satadeep Bhattacharjee https://orcid.org/0000-0002-6717-2881

References

[1] Akerman J 2005 *Science* **308** 508
[2] Ralph D and Stiles M 2008 *J. Mag. Magn. Mater.* **320** 1190
[3] Kawahara T, Ito K, Takemura R and Ohno H 2012 *Microelectron. Reliab.* **52** 613 (advances in non-volatile memory technology)
[4] Khoo K H, Wu G, Jhon M H, Tran M, Ernult F, Eason K, Choi H J and Gan C K 2013 *Phys. Rev.* B **87** 174403
[5] Dieny B and Chshiev M 2017 *Rev. Mod. Phys.* **89** 025008
[6] Beckman O and Lundgren L 1991 *Handbook Magn. Mater.* **6** 181
[7] Fruchart R, Roger A and Senateur J 1969 *J. Appl. Phys.* **40** 1250
[8] Chandra R, Bjarman S, Ericsson T, Häggström L, Wilkinson C, Wäppling R, Andersson Y and Rundqvist S 1980 *J. Solid State Chem.* **34** 389
[9] Catalano A, Arnott R and Wold A 1973 *J. Solid State Chem.* **7** 262
[10] Jernberg P, Yousif A, Häggström L and Andersson Y 1984 *J. Solid State Chem.* **53** 313
[11] Hokabe T, Fujii H, Fujiwara H and Okamoto T 1974 *J. Phys. Soc. Japan* **36** 1704
[12] Zach R, Toboła J, Średniawa B, Kaprzyk S, Casado C, Bacmann M and Fruchart D 2004 *J. Alloys Compd.* **383** 322
[13] Kumar S, Krishnamurthy A and Srivastava B K 2008 *J. Phys. D: Appl. Phys.* **41** 055001
[14] Fujii H, Hōkabe T, Fujiwara H and Okamoto T 1978 *J. Phys. Soc. Japan* **44** 96
[15] Jain S, Kumar S, Krishna P, Shinde A, Krishnamurthy A and Srivastava B K 2007 *J. Alloys Compd.* **439** 13
[16] Dolia S, Krishnamurthy A, Ghose V and Srivastava B K 1993 *J. Phys.: Condens. Matter* **5** 451
[17] Ericsson T, Häggström L, Wäppling R and Methasiri T 1980 *Phys. Scr.* **21** 212
[18] Bhattacharjee S, Bergman A, Taroni A, Hellsvik J, Sanyal B and Eriksson O 2012 *Phys. Rev.* X **2** 011013
[19] Bhattacharjee S, Singh S, Wang D, Viret M and Bellaiche L 2014 *J. Phys.: Condens. Matter* **26** 315008
[20] Bean J J and McKenna K P 2018 *Phys. Rev. Mater.* **2** 125002
[21] Peng S *et al* 2015 *Sci. Rep.* **5** 18173
[22] Blöchl P E 1994 *Phys. Rev.* B **50** 17953
[23] Kresse G and Hafner J 1993 *Phys. Rev.* B **47** 558
[24] Kresse G and Furthmüller J 1996 *Phys. Rev.* B **54** 11169
[25] Perdew J P, Burke K and Ernzerhof M 1996 *Phys. Rev. Lett.* **77** 3865
[26] Ebert K D H and Minar J 2011 *Rep. Prog. Phys.* **74** 096501
[27] Liechtenstein A I, Katsnelson M I, Antropov V P and Gubanov V A 1987 *J. Magn. Magn. Mater.* **67** 65
[28] Skubic B, Hellsvik J, Nordström L and Eriksson O 2008 *J. Phys.: Condens. Matter* **20** 315203
[29] Carlsson B, Gölin M and Rundqvist S 1973 *J. Solid State Chem.* **8** 57
[30] Bhat S S, Gupta K, Bhattacharjee S and Lee S C 2018 *J. Phys.: Condens. Matter* **30** 215401
[31] Kumar S, Chander S, Krishnamurthy A and Srivastava B K 2001 *J. Magn. Magn. Mater.* **237** 135
[32] Maeda Y and Takashima Y 1973 *J. Inorg. Nucl. Chem.* **35** 1963
[33] Scheerlinck D and Legrand E 1978 *Solid State Commun.* **25** 181
[34] Fujii H, Hokabe T, Kamigaichi T and Okamoto T 1977 *J. Phys. Soc. Japan* **43** 41
[35] Zhuravlev I, Antropov V P, Vishina A, van Schilfgaarde M and Belashchenko K D 2017 *Phys. Rev. Mater.* **1** 051401
[36] Evans R F L, Atxitia U and Chantrell R W 2015 *Phys. Rev.* B **91** 144425
[37] Ogiwara M, Iihama S, Seki T, Kojima T, Mizukami S, Mizuguchi M and Takanashi K 2013 *Appl. Phys. Lett.* **103** 242409
[38] Brataas A, Tserkovnyak Y and Bauer G E 2011 *Phys. Rev.* B **84** 054416
[39] Mankovsky S, Ködderitzsch D, Woltersdorf G and Ebert H 2013 *Phys. Rev.* B **87** 014430
[40] Julliere M 1975 *Phys. Lett.* A **54** 225
[41] Ikeda S, Miura K, Yamamoto H, Mizunuma K, Gan H, Endo M, Kanai S, Hayakawa J, Matsukura F and Ohno H 2010 *Nat. Mater.* **9** 721
[42] Khalili Amiri P *et al* 2011 *Appl. Phys. Lett.* **98** 112507
[43] Jiang X, Moriya R and Parkin S 2012 *Appl. Phys. Lett.* **100** 172407
[44] Yang H, Yang S H and Parkin S 2012 *AIP Adv.* **2** 012150
[45] Sinha J *et al* 2013 *Appl. Phys. Lett.* **102** 242405
[46] Wang M *et al* 2018 *Nat. Commun.* **9** 671
[47] Nazir S, Jiang S, Cheng J and Yang K 2019 *Appl. Phys. Lett.* **114** 072407